Research on Gait Optimization of Hexapod Robot Based on Joint Torque and Stability Margin Analysis

Yixuan Han, Tianrui Li, Zhuodong Li*
College of Mechanical Engineering, Yangtze University, Jingzhou, Hubei, China
**Corresponding Author*

Abstract: To address the issues of motion stability and performance enhancement of hexapod biomimetic robots in complex environments, this study focuses on a hexapod robot, combining the D-H modeling method with the Lagrangian dynamics principle to establish an analytical model. Body structure design and typical gait planning are carried out. The feasibility and stability of the gait are verified through simulation analysis, the influence of speed variations on joint torque and stability margin is explored, and relevant kinematic analysis is performed. The results indicate that the hexagonal body layout effectively reduces leg motion interference, and increasing the body size helps improve the static stability margin. Among the gaits, the tripod gait achieves the highest movement speed, while the in-place turning gait is less affected by speed changes and exhibits excellent stability. Increasing the drive torque of the root joint significantly improves the robot's movement speed. This study provides a theoretical reference for the structural design and gait optimization of hexapod biomimetic robots.

Keywords: Hexapod Biomimetic Robot; Structural Design; Gait Planning; Kinematic Analysis

1. Introduction

With the rapid development of embodied intelligence and mobile robot technology, wheeled and tracked robots have been widely applied in structured industrial and urban scenarios. However, in unstructured extreme environments such as earthquake ruins and mountainous forests, their limitations in terrain adaptability, motion stability, and fault tolerance have become increasingly evident, failing to meet the stringent demands of high-risk operations and emergency rescue. To address this challenge, research on hexapod biomimetic robots is of particular importance. By imitating the six-legged structure of insects, these robots combine stability and flexibility[1,2], and with superior terrain adaptability, motion stability, and load capacity, they have become important platforms for environmental detection and task execution[3-5]. Compared with wheeled and tracked robots, hexapod robots can flexibly select ground support points by adjusting their gait, demonstrating stronger adaptability and mobility in complex terrains such as rugged surfaces, gravel, and ravines[6]. However, under external disturbances such as terrain changes, the robot's traveling speed is not constant, which affects its stability. Therefore, studying joint torque and stability margin is of significant reference value in hexapod robot design[7,8]. The motion performance of hexapod robots is influenced by the coupling of multiple factors such as body layout, gait strategy, and joint control. Moreover, the development cycle of physical prototypes is long, expensive, and involves high trial-and-error costs. Hence, conducting precise mechanical design and motion simulation research prior to hardware development holds important engineering guiding significance.

Many scholars have conducted in-depth research on multi-legged robots. Liang [9] investigated the super-twisting algorithm for quadrotor UAVs to enhance their trajectory tracking performance in disturbed flight environments. Based on bionic principles, Men et al.[10] studied an adaptive motion control method for a bio-inspired hexapod robot by drawing on the limb structure and behavioral characteristics of tarantulas. Aiming at the body tilt problem of a hexapod peristaltic climbing robot when moving on steel pile surfaces, Chen et al.[11] proposed a stability control method based on an attitude controller. Yang et al.[12] put forward an innovative leg control scheme through research on mechanical structure design, behavioral

inverse kinematics, and control algorithms.

Most of the above studies focus on attitude compensation and self-stabilization control strategies under complex road disturbances. However, there is still a lack of systematic quantitative analysis on the quantitative correlation between variations in robot travel speed, joint torque distribution of legs[13], and the evolution of stability margin. In practical applications, severe fluctuations in joint torque and abrupt changes in stability margin directly affect walking stability and structural fatigue life, restricting the continuous operation of robots in complex environments.

2. Structural Design of Hexapod Robot

2.1 Body Layout Optimization

The base plate layout of a hexapod robot directly affects leg motion interference and static stability. Common layouts are rectangular and hexagonal, as shown in Figure 1. Motion interference tests show that the rectangular layout causes severe leg motion interference, limiting stride frequency and movement speed. The hexagonal layout features centrally and symmetrically distributed legs, resulting in minimal overlap of leg motion spaces, which significantly improves interference. Furthermore, the hexagonal layout provides an isotropic stability basis, and the anti-overturning capability does not depend on the movement direction, making it suitable for multi-directional motion requirements. Therefore, this paper adopts a hexagonal base plate layout.

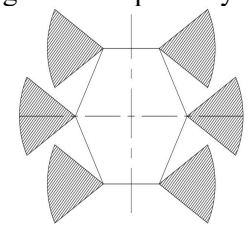

(a)Rectangular Layout

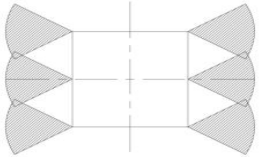

(b)Hexagonal Layout

Figure 1. Two Different base Plate Layouts of the Robot

Static stability margin is an important indicator for measuring the anti-overturning capability of a robot. It is defined as the shortest distance from the projection of the center of gravity onto the support plane to the boundary of the support polygon. Assuming the geometric center of the robot's base plate is the center of gravity, the support plane is constructed using three non-adjacent foot endpoints, and the static stability margin h is the shortest distance from the projection of the center of gravity to the support polygon. Based on the geometric relationship shown in Figure 2, ρ and h are given by:

$$\rho = arctan\left(\frac{\gamma}{2\mu + \alpha + \frac{\beta - \alpha}{2}}\right) \quad (1)$$

$$\hbar = (\mu + 2\beta) \cdot sin\rho \quad (2)$$

where γ is the base plate parameter, μ is the top-view foot length, and α and β are the core dimensions of the body. Fixing γ=100 mm and μ=80 mm, the simulation analysis results shown in Figure 3 indicate that reducing α or increasing β improve the stability margin. However, the value of β must also consider the overall weight, load capacity, and structural coordination. An excessively large β reduces the power-to-weight ratio; therefore, a trade-off between stability and practicality is necessary.

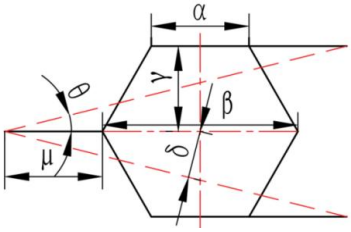

Figure 2. Stability Parameter Diagram

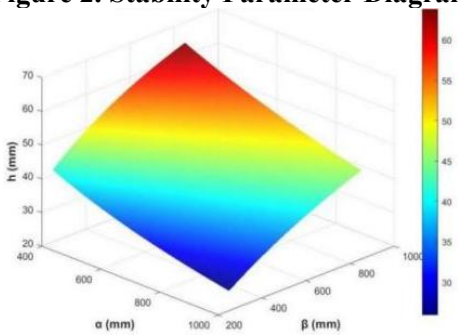

Figure 3. Simulation Analysis Results of Stability Margin and Body Dimensions

2.2 Model Establishment

Based on the hexagonal layout, a three-link leg structure consisting of a coxa, femur, and tibia was designed. The three-link configuration effectively increases the foot-end workspace, allowing the foot-end movement range to be away from the body, improving the ability to traverse complex terrains. The coxa length is

determined based on the basic principle of accommodating the servo installation while avoiding motion space interference between front and rear legs.

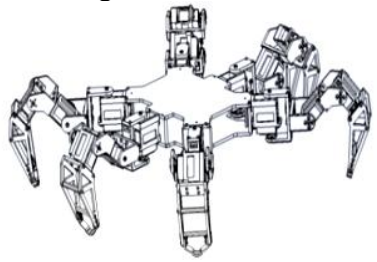

Figure 4. Robot Structure Diagram

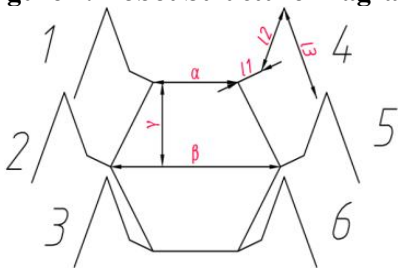

Figure 5. Simplified Structure Diagram

The robot uses an Arduino as the control board and is equipped with sensors for motion control. The left legs are numbered 1, 2, 3 from front to back, and the right legs are 4, 5, 6. The core structural parameters are shown in Table 1. The structure diagram is shown in Figure 4, and the simplified structure is shown in Figure 5.

Table 1. Core Structural Parameters of the Hexapod Robot

Structural Parameter Name	Parameter Value (mm)
Coxa length l_1	80.32
Femur length l_2	78.14
Tibia length l_3	145.13
Front body width α	137.8
Body width β	180
Body length γ	103.9

3. Gait Design of Hexapod Robot

3.1 Core Gait Parameters

To facilitate gait planning and performance evaluation, the following core parameters are defined:

Support phase T_s: The time when the robot's leg contacts the ground and supports the body.

Swing phase T_p: The time when the robot's leg leaves the ground to complete a step;

Gait cycle T: The total time for a leg to complete one support and swing action, $T=T_s+T_p$.

Duty factor φ: The ratio of the support phase to the gait cycle, $\varphi=T_s/T$.

Movement speed V: The ratio of step length S to the support phase time,, $V=S/T_s$.

3.2 Straight-line Gait Planning

The straight-line gaits of hexapod robots are divided into aperiodic and periodic types. Periodic waveform gaits are simple to control and have good stability, making them the preferred gait for flat terrain. Waveform gaits require a uniform duty factor across all legs and prohibit consecutive legs on the same side from being in the swing phase simultaneously, satisfying motion symmetry and stability constraints:

$$\varphi_i=\varphi(i=1,2\cdots6) \tag{3}$$

$$t_i=t_{i+2}+T_p \tag{4}$$

$$t_i=t_{i+1}+\frac{T}{2}(i=1,3,5) \tag{5}$$

Furthermore, the conditions that each leg of the hexapod robot must satisfy when executing a waveform gait are:

$$t_i^n=t_{i+2}^n+T_p(1\le i\le 4) \tag{6}$$

$$t_6^n=t_5^n+\frac{T}{2} \tag{7}$$

t_i^n represents the start time of the nth step of the i-th leg.

From the above equations, we obtain:

$$(1-\varphi)=\frac{T}{T_p} \tag{8}$$

Depending on the duty factor β, waveform gaits can be classified into several types. Among them, the tripod gait ($\varphi=1/2$), tetrapod gait ($\varphi=2/3$), and wave gait ($\varphi=5/6$)are typical gaits with constant support phase states. The performance of the three gaits differs significantly: the tripod gait always has 3 legs supporting at any single moment, providing the fastest movement speed, and is the most common straight-line gait in practical applications; the wave gait has up to 5 legs supporting at any single moment, offering the best stability; the tetrapod gait falls between the two. This paper focuses on the tripod gait, i.e., the gait when φ=1/2.

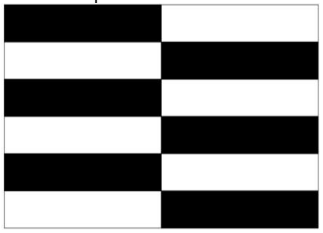

Figure 6. Tripod Gait Timing Diagram

The timing diagram of the tripod gait within one cycle is shown in Figure 6. When the hexapod robot moves, the six feet do not swing simultaneously to achieve linear motion. Instead, they are divided into two groups. The lines connecting the contact points of the feet in the swinging and supporting states with the ground form a triangle, hence it is called the tripod gait[14]. According to the formula, the robot's movement speed is related to the step length and the duration of the support phase. If the step length S is the same for various gaits, the movement speed V is inversely proportional to T_s and is inversely proportional. Therefore, the tripod gait achieves the fastest movement speed and is the most common in practical design.

4. Kinematic Analysis of Hexapod Robot

4.1 Single Leg Forward Kinematics Analysis

The D-H modeling method is used to model the kinematics of the single-leg three-link mechanism. The base coordinate system O_0 and joint coordinate systems O_1–O_4 are established.

Table 2. Single Leg D-H Parameter Table

Link	a_{i-1}	α_{i-1}	d_i	θ_i
1	0	0°	0	θ_1
2	l_1	90°	0	θ_2
3	l_2	0°	0	θ_3
4	l_3	0°	0	0

Based on the D-H transformation matrix, the coordinate transformation matrix between adjacent joints is derived. Substituting each parameter yields the total transformation matrix of the end coordinate system O_4 relative to the base coordinate system O_0 , and finally the position equation of the foot end relative to the joint base coordinate system is obtained:

The transformation matrix between the i-1th joint and the i-th joint is:

$$ {}_{i}^{i-1}T = \begin{bmatrix} \cos\theta_i & -\sin\theta_i & 0 & \alpha_{i-1} \\ \cos\alpha_{i-1}\sin\theta_i & \cos\alpha_{i-1}\cos\theta_i & -\sin\alpha_{i-1} & -d_i\sin\alpha_{i-1} \\ \sin\alpha_{i-1} & \sin\alpha_{i-1}\cos\theta_i & \cos\alpha_{i-1} & d_i\cos\alpha_{i-1} \\ 0 & 0 & 0 & 1 \end{bmatrix} \tag{9} $$

Substituting the parameters from Table 2 into the above formula, the transformation matrix of the end coordinate system relative to the base coordinate system is:

$$ {}_{0}^{4}T = \begin{bmatrix} \cos\theta_1\cos(\theta_2+\theta_3) & -\cos\theta_1\sin(\theta_2+\theta_3) & \sin\theta_1 & l_3\cos\theta_1\cos(\theta_2+\theta_3)+\cos\theta_1(l_2\cos\theta_2+l_1) \\ \sin\theta_1\cos(\theta_2+\theta_3) & -\sin\theta_1\sin(\theta_2+\theta_3) & -\cos\theta_1 & l_3\sin\theta_1\cos(\theta_2+\theta_3)+\sin\theta_1(l_2\cos\theta_2+l_1) \\ \sin(\theta_2+\theta_3) & \cos(\theta_2+\theta_3) & 0 & l_3\sin(\theta_2+\theta_3)+l_2\sin\theta_2 \\ 0 & 0 & 0 & 1 \end{bmatrix} \tag{10} $$

The position of the foot end relative to the joint base coordinate system is:

$$ \begin{bmatrix} p_x \\ p_y \\ p_z \end{bmatrix} = \begin{bmatrix} c_1c_{23}l_3 + c_1(c_2l_2 + l_1) \\ s_1c_{23}l_3 + s_1(c_2l_2 + l_1) \\ s_{23}l_3 + s_2l_2 \end{bmatrix} \tag{11} $$

Where $c_m = \cos\theta_m$, $s_m = \sin\theta_m$, $c_{23} = \cos(\theta_2 + \theta_3)$, $s_{23} = \sin(\theta_2 + \theta_3)$

4.2 Single Leg Inverse Kinematics Analysis

Forward kinematics solves the foot-end position coordinates relative to the coxa given the joint angles, while inverse kinematics analysis aims to determine each joint angle given the desired foot-end pose. Assuming the foot-end pose matrix is T, the inverse D-H transformation matrices are left-multiplied to establish a system of equations relating the foot-end position and joint angles, yielding the angle equations for the root joint θ_1, hip joint θ_2, and knee joint θ_3:

Assuming the foot-end pose is:

$$ T = \begin{bmatrix} n_x & o_x & a_x & x \\ n_y & o_y & a_y & y \\ n_z & o_z & a_z & z \\ 0 & 0 & 0 & 1 \end{bmatrix} \tag{12} $$

By left-multiplying the inverse matrices respectively, we obtain:

$$ {}_{1}^{0}T^{-1} \times {}_{4}^{0}T = {}_{2}^{1}T \times {}_{3}^{2}T \times {}_{4}^{3}T \tag{13} $$

$$ {}_{2}^{1}T^{-1} \times {}_{1}^{0}T^{-1} \times {}_{4}^{0}T = {}_{3}^{2}T \times {}_{4}^{3}T \tag{14} $$

Expanding (13) and (14) allows establishing the system of equations:

$$ \begin{cases} -s_1p_x + c_1p_y = 0 \\ c_2(c_1p_x + s_1p_y) + s_2p_z - c_2l_1 = c_3l_3 + l_2 \\ -s_2(c_1p_x + s_1p_y) + c_2p_z + s_2l_1 = s_3l_3 \end{cases} \tag{15} $$

Solving yields the root joint angle, hip joint angle, and knee joint angle as follows:

$$ \begin{cases} \theta_1 = \arctan(\dfrac{x}{y}) \\ \theta_2 = \arccos\dfrac{p_z}{\sqrt{O^2 + p_z^3}} - \gamma \\ \theta_3 = -\arccos\dfrac{Oc_2 + p_zs_2 - l_2}{l_3} \end{cases} \tag{16} $$

$$O=(c_1p_x+s_1p_y-l_1),\gamma=\arcsin\frac{O^2+p_z^2+l_2^2+l_3^2}{\sqrt{4l_2(O^2+p_z^2)}} \quad (17)$$

Through inverse kinematics analysis, the goal of deriving joint motion from the foot-end trajectory is achieved, providing a theoretical basis for joint servo control.

5. Simulation Analysis and Experimental Verification

5.1 Foot-End Workspace and Trajectory Planning Simulation

MATLAB was used to simulate the foot-end workspace. The ranges were set as root joint $\theta_1\in[-45°, 45°]$, hip joint $\theta_2\in[-35°, 95°]$, knee joint $\theta_3\in[-125°, 35°]$,Substituting the structural parameters yielded the foot-end reachable space. The simulation results of the foot-end workspace are shown in Figure 7, and its projections onto the X-Y, X-Z, and Y-Z planes are presented in Figures 8 to Figure 10, respectively. The foot-end workspace is symmetrical in the X-Y and Y-Z planes, and the space below the X-Z plane is larger than above, consistent with the actual motion characteristics, verifying the correctness of the forward kinematics analysis.

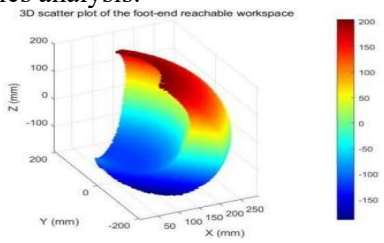

Figure 7. Foot-end Reachable Space

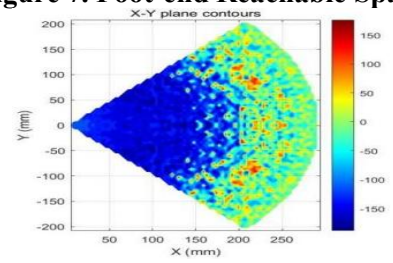

Figure 8. X-Y Plane Projection Contour

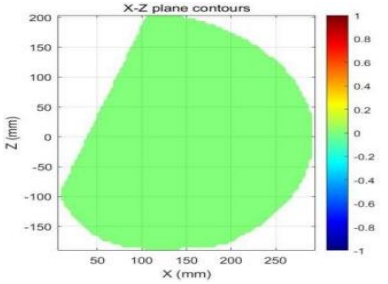

Figure 9. X-Z Plane Projection Contour

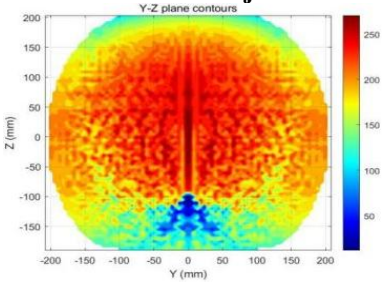

Figure 10. Y-Z Plane Projection Contour

5.2 Foot-end Trajectory Planning

To ensure smooth motion during the swing phase and reduce impact at touchdown, a seventh-degree polynomial is used for foot-end trajectory planning. Compared to the fifth-degree polynomial, the seventh-degree polynomial can simultaneously constrain the position, velocity, and acceleration at the start and end points, making the acceleration of the foot end zero at the lift-off and touchdown moments, further reducing impact.

Assume the hexapod robot moves forward along the x-axis, using the tripod gait, i.e. $\varphi=1/2$. Set the leg lift height $H=60\ mm$, step length $L=100$ mm, and gait cycle $T=1\ s$. Under the tripod gait, the swing phase time is $Tp=T/2=0.5\ s$.

In the x-direction, the constraints are: at $t= 0, x= -L/2, \dot{x}= 0, \ddot{x}= 0$. at $t= T/4, x= 0, \dot{x}= 4L/T$. at $t= T/2, x= L/2, \dot{x}= 0, \ddot{x}= 0$.

In the z-direction, in addition to the start and end point constraints, the leg lift height H is constrained. Solving for the seventh-degree polynomial coefficients yields the swing phase trajectory equations:

$$x(t)=L\times\left(-\frac{1}{2}+560\left(\frac{t}{T}\right)^4-2688\left(\frac{t}{T}\right)^5+4480\left(\frac{t}{T}\right)^6-2560\left(\frac{t}{T}\right)^7\right) \quad (18)$$

$$z(t)=H\times\left(64\left(\frac{2t}{T}\right)^3-192\left(\frac{2t}{T}\right)^4+192\left(\frac{2t}{T}\right)^5-64\left(\frac{2t}{T}\right)^6\right) \quad (19)$$

This equation ensures that the velocity and acceleration of the foot end are zero at the start and end points of the swing phase, and the maximum leg lift height H is reached at the midpoint $t=T/4$ of the swing phase, meeting the smoothness requirements for foot-end motion.

When the foot end is in the support phase, its trajectory can be approximated as a straight line parallel to the x-axis. The foot end is stationary relative to the ground and moves backward uniformly relative to the body to ensure the body moves forward uniformly. The trajectory during

the support phase can be expressed by the linear equation:

$$x(t) = L \times \left(-\frac{1}{2} + 560\left(\frac{t}{T}\right)^4 - 2688\left(\frac{t}{T}\right)^5 + 4480\left(\frac{t}{T}\right)^6 - 2560\left(\frac{t}{T}\right)^7 \right) \quad \left(t \in \left[0, \frac{T}{2}\right]\right) \tag{20}$$

To verify the correctness of the calculations, a MATLAB simulation was conducted to compare the displacement, velocity, and acceleration in the x-direction between the seventh-degree and fifth-degree polynomials, as illustrated in Figure 11 to Figure 13, respectively. The foot-end trajectory in the X-Z plane is shown in Figure 14. The results demonstrate that the displacement, velocity, and acceleration curves of the seventh-degree polynomial transition smoothly at the start and end points, which helps reduce impact during foot lift-off and touchdown. Additionally, installing a buffer pad at the robot's foot end can further mitigate oscillation and improve walking stability.

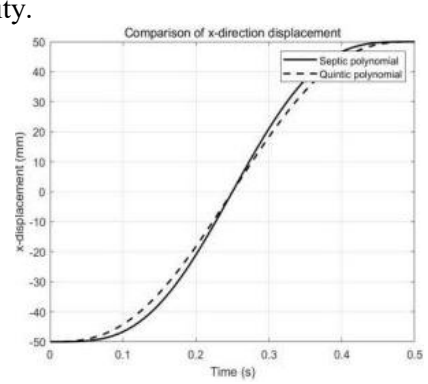

Figure 11. X-Direction Displacement Comparison

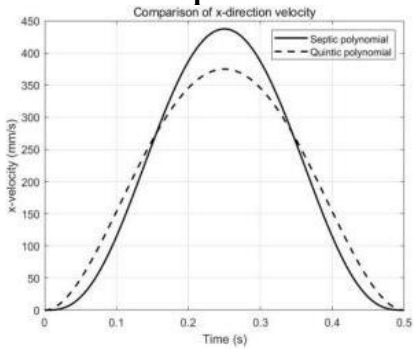

Figure 12. X-Direction Velocity Comparison

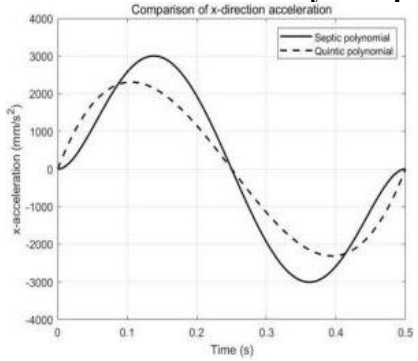

Figure 13. X-direction Acceleration Comparison

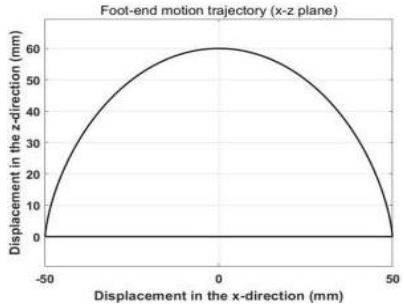

Figure 14. Foot-End Trajectory

5.3 Simulation of Joint Torque and Speed Correlation

A kinematic model of the hexapod robot was built in the MATLAB Simulink environment. Based on the Lagrangian dynamics principle, the kinetic-potential energy model of the swing leg's RRR open-chain mechanism was established. The Lagrangian function is:

$$L \equiv K_1 + K_2 + K_3 - P_1 - P_2 - P_3 \tag{21}$$

The joint drive torque is solved by combining it with the second kind of Lagrangian equation:

$$T_i = \frac{d}{dt}\left(\frac{\partial L}{\partial \dot{q}_i}\right) - \frac{\partial L}{\partial q_i} \tag{22}$$

Where K is the link kinetic energy, P is the link potential energy, and q_i is the joint angular displacement.

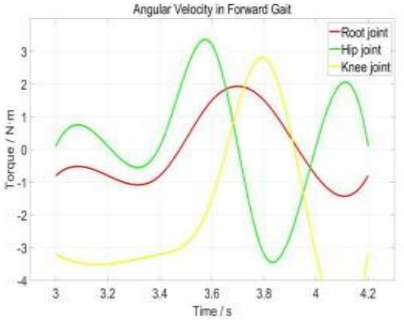

Figure 15. Single Leg Joint Torque Variation Curve

With swing step lengths set to 85 mm, 100 mm, and 115 mm (corresponding to different movement speeds), the simulation results are presented in Figure 15 to Figure 18. The variation in joint torque during a single swing phase can be summarized as follows: (1) The robot's movement speed is positively correlated with the root joint drive torque, meaning that increasing the root joint drive torque effectively enhances movement speed. (2) The maximum torque required by the hip joint approaches 1 N·m, which is considerably higher than that of

the root joint and knee joint, establishing the hip joint as a critical component for ensuring stable motion of the swing leg.

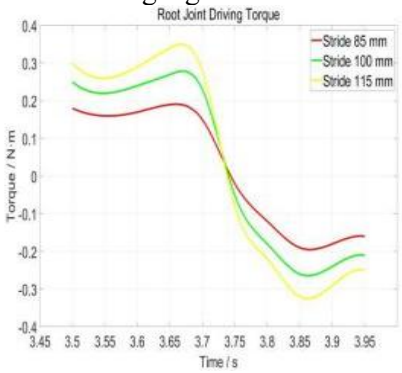

Figure 16. Root Joint Drive Torque

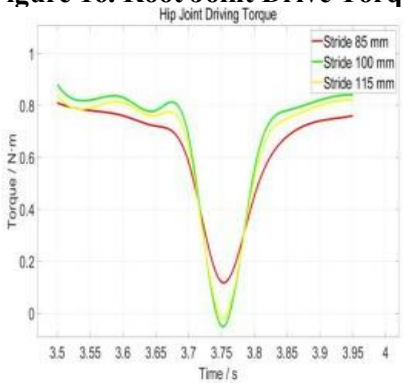

Figure 17. Hip Joint Drive Torque

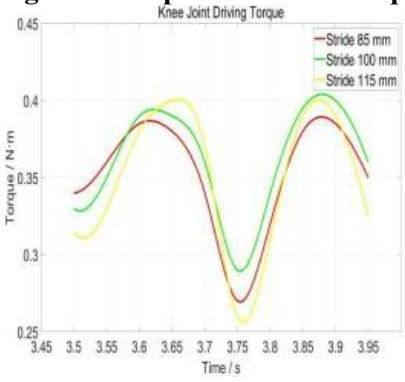

Figure 18. Knee Joint Drive Torque

5.4 Physical Experiment Verification

Based on the simulation results, a physical prototype of the hexapod robot was developed. The gait and joint control data were loaded into the hardware driver, and an in-place clockwise turning experiment was conducted. The experimental parameters were set as follows: leg lift height 60 mm, gait cycle 1s, duty factor φ=1/2 . The experimental process is shown in Figure 19. The robot moved smoothly during the turning process, without obvious tipping, jerking, or foot dragging. The actual motion trajectory was basically consistent with the simulation expectations. The experiment verified the feasibility of the designed structural scheme, gait strategy, and control method, indicating that the simulation results have engineering guiding value.

Figure 19. Tripod Gait In-Place Turning

6. Conclusion

This paper conducts research on the structural design and gait optimization of hexapod biomimetic robots. Through theoretical analysis, modeling, simulation verification, and physical verification, the following main conclusions are drawn:

(1) Structural optimization: The hexagonal body layout effectively reduce leg motion interference. The static stability margin increases with decreasing body dimensing α and increasing β. The structural design requires a trade-off between stability and overall robot weight to select the optimal parameters.

(2) Gait performance: Among straight-line gaits, the tripod gait (φ=1/2) achieves the fastest movement speed and is the optimal choice for flat terrain. The in-place turning gait is less affected by speed changes, and its stability is significantly better than that of the lateral gait, making it suitable for obstacle avoidance in complex environments.

(3) Joint torque characteristics: The robot's movement speed is positively correlated with the root joint drive torque, which is a key control parameter for speed enhancement. The hip joint exhibits the highest torque peak, requiring matching high-torque servos to ensure the stability of the swing leg motion.

(4) Trajectory planning and verification: The

foot-end trajectory planning method combining the seventh-degree polynomial and linear equation effectively ensure swing phase smoothness and reduce touchdown impact. physical prototype experiments verified the feasibility of the structural scheme and gait strategy.

This study provides a theoretical basis and engineering reference for the structural parameter design and gait control strategy optimization of hexapod biomimetic robots. Future work will focus on gait adaptive control in unstructured terrains and real-time obstacle avoidance strategies based on visual perception to further enhance the robot's adaptability to complex environments.

Acknowledgments

This research was supported by the Yangtze University Undergraduate Innovation and Entrepreneurship Training Program project "Design of a Bionic Articulated Hexapod Robot" (Grant No.: Yz2024144), for which we are sincerely grateful. We would also like to thank the supervising instructor for their valuable guidance and the team members for their collaborative support.

References

[1] Fu X, Zheng Y, Ma S J, et al. Technological Innovation of Intelligent Hexapod Robots in Outdoor Detection Field. Information Recording Materials, 2025, 26(09): 36-38.

[2] Zrnic N D, Gasic V M, Bonsjak S M. Dynamic responses of a gantry crane system due to a moving body considered as moving oscillator. Archives of Civil & Mechanical Engineering, 2015, 15(1):243-250.

[3] Chen S Q, Li S Y, Lu Z G, et al. Review of Key Technologies for Hexapod Robots. Mechanical & Electrical Engineering Technology, 2022, 51(11): 146-152.

[4] Sun H C, He L L, Jiang W W, et al. Development of Hexapod Robot Based on Bionic Principle. Technology Innovation and Application, 2024, 14(30): 32-35.

[5] Zhang J Z, Jin Z L, Zhao Y M. Dynamics analysis ofleg mechanism of six-legged firefighting robot. Journal of Mechanical Science and Technology, 2018, 32(1): 351-361.

[6] Li Tao, Cai Jing, Jin Junyi, et al. Gait Design and Motion Study of Hexapod Bionic Robot. Mechanical Science and Technology, 2024, 43(9):1685-1695.

[7] Salehian A, Seigle RT M, Inman D J. Dynamic effects of a radar panel mounted on a truss satellite. AIAA Journal, 2007, 45(7):1642-1654.

[8] Wang Y Z, Wang Y C. Motion Structure Design and Simulation Analysis of a Linkage-type Hexapod Mobile Robot. Mechanical Engineer, 2026, (02): 143-146.

[9] Liang Hongji, Li Junli, Zhu Xiaoying, et al. Trajectory Tracking Control of Quadrotor UAV Based on Fast Adaptive Super-Twisting Sliding Mode Algorithm. Control Engineering, 1-9[2026-04-08]. https://doi.org/10.14107/j.cnki.kzgc.20240269.

[10] Men Tingfeng, Cao Le, Xu Haoyang, et al. Adaptive Motion Control Method for Biomimetic Hexapod Robot Based on Fusion Gait. Chinese Journal of Medical Physics, 2025, 42(10): 1374-1383.

[11] Chen K Y, Chang J Y, Sheng C Y, et al. Attitude Control of Hexapod Creeping Climbing Robot Based on Fuzzy Control. Journal of Heilongjiang University of Science and Technology, 2026, 36(01): 122-128.

[12] Yang Yubin, Gao Qiang, Guo Wenguang. Research on Leg Control of Hexapod-Tracked Composite Robot//Smart Information Processing Industrialization Branch of China High-Tech Industrialization Research Association, National Key Laboratory of Space-Based Intelligent Information Processing, Editorial Office of Computer Engineering and Applications. Proceedings of the 19th National Conference on Signal and Intelligent Information Processing and Application. School of Information Science and Technology, Beijing University of Technology; Beijing Houtai Intelligent Technology Co., Ltd., 2025: 140-144.

[13] Ma Xiufeng, Zhang Qifeng, Sun Yingzhe. Gait Design and Motion Simulation of Biomimetic Hexapod Robot. Computer Simulation, 2023, 40(02): 255-260+269.

[14] Zhang Y J, Yang Y K, Xiao Z X, et al. Dynamic Simulation Analysis of Hexapod Ant Bionic Robot. Machinery Design & Manufacture, 2024, (11): 83-87.

